

Magnetic moments of open bottom–charm molecular pentaquark octets

Halil Mutuk^{1,*} and Xian-Wei Kang^{2,†}

¹*Department of Physics, Faculty of Sciences, Ondokuz Mayıs University, 55200 Samsun, Türkiye*

²*Key Laboratory of Beam Technology of the Ministry of Education,
School of Physics and Astronomy, Beijing Normal University, Beijing 100875, China*

We present a comprehensive theoretical investigation of the magnetic moments of open heavy-flavor molecular pentaquarks with quark compositions $b\bar{c}qqq$ and $c\bar{b}qqq$ (where $q = u, d, s$). Employing a molecular picture in which the pentaquarks are treated as S-wave bound states of a heavy baryon and a meson, we systematically construct the complete spin–flavor wavefunctions for the two distinct $SU(3)_f$ octet representations, 8_{1f} and 8_{2f} , arising from symmetric and antisymmetric light-diquark configurations, respectively. Within the framework of the constituent quark model, we calculate the magnetic moments of spin-parity configurations, $J^P = \frac{1}{2}^- (\frac{1}{2}^+ \otimes 0^-)$ and $J^P = \frac{1}{2}^-, \frac{3}{2}^- (\frac{1}{2}^+ \otimes 1^-)$, for each member of the $b\bar{c}$ and $c\bar{b}$ octets. Our results reveal a striking hierarchy: in the 8_{2f} representation, the $\frac{1}{2}^+ \otimes 0^-$ states exhibit near-universal magnetic moments ($\mu \approx -0.062 \mu_N$ for $b\bar{c}qqq$ and $\mu \approx +0.362 \mu_N$ for $c\bar{b}qqq$), as a direct consequence of the spin-singlet light-diquark that suppresses light-quark contributions. In contrast, the 8_{1f} representation shows a broad spectrum of values with frequent sign changes, reflecting the active role of the symmetric light-diquark. The clear differences between the $b\bar{c}$ and $c\bar{b}$ families demonstrate explicit heavy-quark flavor symmetry breaking in electromagnetic observables. These predictions provide a detailed set of electromagnetic benchmarks that can serve as discriminants for the internal flavor structure and spin configuration of future experimentally observed open heavy-flavor pentaquarks, offering valuable guidance for ongoing and future searches at facilities such as LHCb and Belle II.

I. INTRODUCTION

The landscape of hadron spectroscopy has been profoundly reshaped by the discovery of exotic multi-quark states, challenging the traditional meson and baryon configurations and offering new insights into the nonperturbative regime of Quantum Chromodynamics (QCD). The first landmark evidence for exotic hidden-charm pentaquark states was reported by the LHCb Collaboration in 2015 through the analysis of the $J/\psi p$ invariant-mass distribution in the decay channel $\Lambda_b^0 \rightarrow J/\psi K^- p$ [1]. Two resonant structures, $P_c(4380)^+$ and $P_c(4450)^+$, were identified. These findings constituted the first unambiguous observation of pentaquark candidates containing hidden-charm ($c\bar{c}uud$) and marked the beginning of a new era in the experimental exploration of multi-quark hadrons.

Building upon this discovery, the LHCb Collaboration performed an updated amplitude analysis in 2019, revealing three distinct hidden-charm pentaquark states: $P_c(4312)^+$, $P_c(4440)^+$, and $P_c(4457)^+$ [2]. The previously observed broad $P_c(4450)^+$ resonance was resolved into two narrower states, $P_c(4440)^+$ and $P_c(4457)^+$. Following the convention for naming exotic hadrons [3], these three states are now denoted as

$$P_c(4312) \rightarrow P_\psi^N(4312), \quad P_c(4440) \rightarrow P_\psi^N(4440), \quad P_c(4457) \rightarrow P_\psi^N(4457). \quad (1)$$

Further evidence for hidden-charm pentaquarks containing strangeness was reported by the LHCb Collaboration in 2021. A neutral resonance, $P_{cs}(4459)^0$ (denoted as $P_{\psi_s}^\Lambda(4459)$ in the updated nomenclature), was found in the $J/\psi \Lambda$ invariant-mass distribution of the decay $\Xi_b^- \rightarrow J/\psi K^- \Lambda$, with a local significance of 3.1σ including systematic uncertainties [4]. Independent evidence for the same state, with a local significance of 3.3σ , has subsequently been reported by the Belle Collaboration in $\Upsilon(1S, 2S)$ inclusive decays to $J/\psi \Lambda$, yielding a mass of $(4471.7 \pm 4.8 \pm 0.6) \text{ MeV}/c^2$ and a width of $(21.9 \pm 13.1 \pm 2.7) \text{ MeV}$ [5]. More recently, another strange hidden-charm pentaquark, $P_{cs}(4338)^0$ (or $P_{\psi_s}^\Lambda(4338)$), was observed by LHCb in the decay $B^- \rightarrow J/\psi \Lambda \bar{p}$ [6].

Although the quantum numbers of these strange hidden-charm pentaquarks have not yet been experimentally determined, the preferred assignments suggested by amplitude analyses and by molecular interpretations are $J^P = \frac{3}{2}^-$ for $P_{\psi_s}^\Lambda(4459)$ and $J^P = \frac{1}{2}^-$ for $P_{\psi_s}^\Lambda(4338)$ [4, 6–9]. These assignments do not follow from a generic spin–mass ordering: the two states are widely interpreted as molecules associated with *different* meson–baryon channels, $\bar{D}^* \Xi_c$

* hmutuk@omu.edu.tr

† xwkang@bnu.edu.cn

for $P_{\psi_s}^\Lambda(4459)$ and $\bar{D}\Xi_c$ for $P_{\psi_s}^\Lambda(4338)$, with thresholds at ≈ 4477 and ≈ 4336 MeV, respectively. The mass gap between the two candidates therefore reflects the gap between these underlying thresholds, not a hyperfine splitting; the same logic underlies our treatment of open bottom–charm pentaquarks below.

The discovery of hidden-charm pentaquarks has ignited a vibrant theoretical and experimental program. Significant progress has been made on magnetic moments in the hidden-charm sector [10–25] and, to a lesser extent, in the hidden-bottom sector [26, 27]. By contrast, pentaquarks containing both bottom (b) and charm (c) quarks — with compositions $b\bar{c}qqq$ or $\bar{c}bqqq$ — constitute a unique and relatively unexplored class of mixed heavy-flavor exotics that probes QCD dynamics in an intermediate mass regime. A complete color–magnetic $SU(3)_f$ classification of such heavy pentaquark multiplets was established in Ref. [28]. Coupled-channel unitary analyses based on the local hidden-gauge approach have shown that meson–baryon interactions in the $\bar{c}bqqq$ and $b\bar{c}qqq$ systems dynamically generate multiple open-heavy resonances [29], and an extended local hidden-gauge study of $cc\bar{q}qs$, $bb\bar{q}qs$ and $bc\bar{q}qs$ systems has identified fourteen S-wave molecular candidates, including narrow bottom–charm states relevant to the present work [30].

The magnetic moment is a fundamental electromagnetic property that encodes the distribution of charge and spin among a hadron’s constituents. For pentaquarks, it depends sensitively on the relative alignment of heavy- and light-quark spins, the orbital configuration, and the overall color–flavor symmetry, and can therefore differ markedly across structural models even for states with similar masses and quantum numbers. This sensitivity makes the magnetic moment a powerful discriminant of the internal architecture of exotic hadrons, and is especially valuable in the bottom–charm case where the interplay of two distinct heavy quarks and three light quarks provides a richer structure than in single-heavy-flavor systems.

From an experimental standpoint, the search for bottom-charm pentaquarks is entering a promising era. The upgraded LHCb experiment and Belle II are accumulating large statistics in heavy-flavor channels and can probe several plausible production mechanisms (fragmentation, photoproduction), with discovery channels such as B_c plus light hadrons, $J/\psi\Lambda_b$, or $D^{(*)}\Sigma_b$. Although no bottom-charm pentaquark has been reported to date, theoretical guidance on their expected masses, widths, and distinguishing properties — in particular their magnetic moments — is essential to sharpen these searches and, in the event of a candidate, to elucidate its internal structure.

In this work, we focus specifically on bottom–anticharm (and charm–antibottom) pentaquarks within the molecular model, concentrating on the two distinct $SU(3)_f$ octet representations, 8_{1f} and 8_{2f} , which originate from symmetric and antisymmetric light–diquark configurations in the baryon component. This framework provides a well-defined and computationally tractable approach for constructing pentaquark wave functions while respecting color confinement and Pauli statistics. In this picture, open bottom–charm pentaquarks are described as hadronic molecules composed of a singly heavy baryon and heavy–light meson, namely $(bqq)(\bar{c}q)$ for the $b\bar{c}$ sector and $(cqq)(\bar{b}q)$ for the $\bar{c}b$ sector. The interaction between these two hadrons is assumed to generate loosely bound states, predominantly in an S-wave configuration.

Throughout this work we denote the eight members of each open bottom–charm pentaquark octet by $P_{b\bar{c}}^i$ and $P_{\bar{c}b}^i$ ($i = 1, \dots, 8$), following the compact labelling adopted in the *Review of Particle Physics* [31] and in previous theoretical studies of $bc\bar{q}qq$ and $\bar{b}cqqq$ systems [28–30]. We emphasize that no exotic-hadron name has yet been assigned within the LHCb convention [3] to any open bottom–charm pentaquark, simply because no such state has so far been experimentally observed. Should a candidate be reported in the future, the corresponding name in the LHCb scheme would take the form $P_{b\bar{c}}^N$ (for non-strange, isospin-doublet partners), $P_{b\bar{c}}^\Sigma$ or $P_{b\bar{c}}^\Lambda$ (for singly-strange members, depending on the light-quark isospin), and analogously for the $\bar{c}b$ family. The compact symbols $P_{b\bar{c}}^i$, $P_{\bar{c}b}^i$ used in the tables and figures of this paper are adopted purely for notational economy and do not preempt the LHCb naming convention.

The paper is organized as follows. Section II introduces the wave functions in the molecular picture, including the $SU(3)_f$ flavor wave functions and explicit spin wave functions. Section III presents the magnetic moment formalism and its application to the pentaquark octets. Section IV contains the numerical results and their physical interpretation. Section V summarizes our conclusions.

II. WAVE FUNCTIONS

The electromagnetic structure of a hadron is determined by the internal configuration of its constituent quarks. For the open-flavor molecular pentaquarks considered in this work, the total wave function factorizes into flavor, spin, color, and spatial components,

$$\Psi = \psi_{\text{flavor}} \otimes \chi_{\text{spin}} \otimes \xi_{\text{color}} \otimes \eta_{\text{space}}. \quad (2)$$

Fermi-Dirac statistics require the full wave function to be antisymmetric under exchange of identical light quarks. In the molecular picture, this constraint is already satisfied within each constituent hadron. The baryon (Qqq) contains

two identical light quarks (in some flavor configurations), and its color-flavor-spin wavefunction is appropriately antisymmetrized. The meson ($q\bar{Q}'$) contains no identical quarks. When these two color-singlet hadrons bind to form a molecule, there is no additional antisymmetrization required across different hadrons, as the quarks are confined to distinct spatial regions. The spatial part η_{space} for the ground-state S-wave molecule is symmetric, and the color wavefunction ξ_{color} is simply the product of the two individual color singlets, which is overall symmetric.

A clarification regarding the role of the spatial component η_{space} in Eq. (2) is in order. In the non-relativistic constituent quark model, the magnetic-moment operator $\hat{\mu} = \sum_i (Q_i/2M_i) \hat{\sigma}_i$ acts only on the spin-flavor degrees of freedom of the individual quarks and carries no explicit spatial dependence. Consequently, the diagonal magnetic moment of a molecular state factorizes as

$$\langle \Psi | \hat{\mu}_z | \Psi \rangle = \langle \eta_{\text{space}} | \eta_{\text{space}} \rangle \langle \chi_{\text{spin}} \psi_{\text{flavor}} \xi_{\text{color}} | \hat{\mu}_z | \chi_{\text{spin}} \psi_{\text{flavor}} \xi_{\text{color}} \rangle, \quad (3)$$

and since the spatial wave function is normalized, $\langle \eta_{\text{space}} | \eta_{\text{space}} \rangle = 1$, it contributes no overall factor to the result. The diagonal (static) magnetic moments computed in this work are therefore insensitive to the detailed shape of η_{space} and, in particular, are *not* suppressed by the small inter-hadron spatial overlap that characterizes a loosely bound molecular configuration. Spatial-overlap effects do become important for *off-diagonal* transition matrix elements $\langle \Psi' | \hat{\mu}_z | \Psi \rangle$ between molecules of different hadronic content, which are relevant for radiative-decay widths; we return to this point in Sec. IV. The factorization adopted here is the standard prescription used throughout the constituent-quark-model literature on molecular pentaquarks [14, 19, 20, 22, 26, 27].

In the molecular interpretation, open-bottom-charm pentaquarks arise from a singly heavy baryon and a heavy-light meson of the form $(Qqq)(\bar{Q}'q)$, with $(Q, Q') = (b, c)$ or (c, b) . In principle, the same valence quark content $\bar{Q}'Qqqq$ admits a second hadronic decomposition, namely a light octet baryon combined with a heavy-heavy meson, $(qqq)(Q\bar{Q}')$, which for the open bottom-charm system corresponds to channels of the type $NB_c^{(*)}$, $\Lambda B_c^{(*)}$, $\Sigma B_c^{(*)}$, or $\Xi B_c^{(*)}$. We do not consider this configuration in the present work, for the following physical reason. Molecular binding in the meson-baryon sector is governed predominantly by light-meson exchange (one-pion, ρ , ω , σ) and by light-quark rearrangement between the constituent hadrons. The $B_c^{(*)}$ meson, however, is an SU(3) flavor singlet containing no light quarks; consequently the $B_c B_c \pi$, $B_c B_c \rho$, $B_c B_c \omega$, and $B_c B_c \sigma$ vertices vanish at tree level, and the residual interaction with a light baryon is restricted to heavy-meson exchange and multi-pion or gluonic channels, all of which are strongly suppressed. As a result, the $(qqq)(Q\bar{Q}')$ configuration is not expected to generate dynamically bound molecular states, and is consistently excluded from the coupled-channel analyses of Refs. [29, 30] on which the present molecular assignment is based. We therefore focus exclusively on the $(Qqq)(\bar{Q}'q)$ class, which provides the only molecular configurations supported by the dynamical studies in the literature.

The flavor structure of the singly heavy baryon is governed by the SU(3) flavor symmetry of the two light quarks. Symmetric light-diquark configurations,

$$\{q_1 q_2\} = \frac{1}{\sqrt{2}}(q_1 q_2 + q_2 q_1), \quad (4)$$

belong to the sextet representation 6_f , while antisymmetric diquarks,

$$[q_1 q_2] = \frac{1}{\sqrt{2}}(q_1 q_2 - q_2 q_1), \quad (5)$$

belong to the antitriplet representation $\bar{3}_f$. Combining the baryon with a heavy antimeson ($q\bar{Q}'$) in the 3_f representation generates

$$6_f \otimes 3_f = 10_f \oplus 8_{1f}, \quad (6)$$

$$\bar{3}_f \otimes 3_f = 8_{2f} \oplus 1_f, \quad (7)$$

yielding the overall three-light-quark decomposition

$$3 \otimes 3 \otimes 3 = 1 \oplus 8_1 \oplus 8_2 \oplus 10. \quad (8)$$

Thus, two distinct SU(3) $_f$ flavor octets arise from Eqs. (5)–(6): 8_{1f} , built from symmetric light diquarks via $6_f \otimes 3_f$, and 8_{2f} , built from antisymmetric light diquarks via $\bar{3}_f \otimes 3_f$. In the present work we restrict our analysis to these two octet representations, for three concurrent reasons. First, all experimentally established hidden-charm pentaquark candidates — $P_\psi^N(4312)$, $P_\psi^N(4440)$, $P_\psi^N(4457)$, $P_{\psi s}^\Lambda(4459)$, and $P_{\psi s}^\Lambda(4338)$ — have been classified phenomenologically within SU(3) $_f$ octet multiplets [22, 28]. Second, the coupled-channel dynamical analyses of Refs. [29, 30], which provide the underlying motivation for treating open bottom-charm pentaquarks as hadronic molecules, identify the

TABLE I. Fully explicit spin-flavor wave functions of the $b\bar{c}$ molecular pentaquark octet. The arrows denote quark spin projections. Here $\{q_1q_2\}$ and $[q_1q_2]$ denote symmetric and antisymmetric light-diquark flavor combinations, respectively.

State	Representation	$\psi_{\text{flavor}} \otimes \chi_{\text{spin}}$
$P_{b\bar{c}}^1$	8_{1f}	$-\sqrt{\frac{1}{3}}[(\{ud\}b) \otimes \frac{1}{\sqrt{6}}(\uparrow\downarrow\uparrow + \downarrow\uparrow\uparrow - 2\uparrow\uparrow\downarrow)][(u\bar{c}) \otimes \frac{1}{\sqrt{2}}(\uparrow\downarrow - \downarrow\uparrow)]$ $+\sqrt{\frac{2}{3}}[(\{uu\}b) \otimes \frac{1}{\sqrt{6}}(\uparrow\downarrow\uparrow + \downarrow\uparrow\uparrow - 2\uparrow\uparrow\downarrow)][(d\bar{c}) \otimes \frac{1}{\sqrt{2}}(\uparrow\downarrow - \downarrow\uparrow)]$
$P_{b\bar{c}}^1$	8_{2f}	$([ud]b \otimes \frac{1}{\sqrt{2}}(\uparrow\downarrow\uparrow - \downarrow\uparrow\uparrow))(u\bar{c} \otimes \frac{1}{\sqrt{2}}(\uparrow\downarrow - \downarrow\uparrow))$
$P_{b\bar{c}}^2$	8_{1f}	$\sqrt{\frac{1}{3}}[(\{ud\}b) \otimes \frac{1}{\sqrt{6}}(\uparrow\downarrow\uparrow + \downarrow\uparrow\uparrow - 2\uparrow\uparrow\downarrow)][(d\bar{c}) \otimes \frac{1}{\sqrt{2}}(\uparrow\downarrow - \downarrow\uparrow)]$ $-\sqrt{\frac{2}{3}}[(\{dd\}b) \otimes \frac{1}{\sqrt{6}}(\uparrow\downarrow\uparrow + \downarrow\uparrow\uparrow - 2\uparrow\uparrow\downarrow)][(u\bar{c}) \otimes \frac{1}{\sqrt{2}}(\uparrow\downarrow - \downarrow\uparrow)]$
$P_{b\bar{c}}^2$	8_{2f}	$([ud]b \otimes \frac{1}{\sqrt{2}}(\uparrow\downarrow\uparrow - \downarrow\uparrow\uparrow))(d\bar{c} \otimes \frac{1}{\sqrt{2}}(\uparrow\downarrow - \downarrow\uparrow))$
$P_{b\bar{c}}^3$	8_{1f}	$\sqrt{\frac{1}{3}}[(\{us\}b) \otimes \frac{1}{\sqrt{6}}(\uparrow\downarrow\uparrow + \downarrow\uparrow\uparrow - 2\uparrow\uparrow\downarrow)][(u\bar{c}) \otimes \frac{1}{\sqrt{2}}(\uparrow\downarrow - \downarrow\uparrow)]$ $-\sqrt{\frac{2}{3}}[(\{uu\}b) \otimes \frac{1}{\sqrt{6}}(\uparrow\downarrow\uparrow + \downarrow\uparrow\uparrow - 2\uparrow\uparrow\downarrow)][(s\bar{c}) \otimes \frac{1}{\sqrt{2}}(\uparrow\downarrow - \downarrow\uparrow)]$
$P_{b\bar{c}}^3$	8_{2f}	$([us]b \otimes \frac{1}{\sqrt{2}}(\uparrow\downarrow\uparrow - \downarrow\uparrow\uparrow))(u\bar{c} \otimes \frac{1}{\sqrt{2}}(\uparrow\downarrow - \downarrow\uparrow))$
$P_{b\bar{c}}^4$	8_{1f}	$\frac{1}{\sqrt{6}}[(\{us\}b) \otimes \frac{1}{\sqrt{6}}(\uparrow\downarrow\uparrow + \downarrow\uparrow\uparrow - 2\uparrow\uparrow\downarrow)][(d\bar{c}) \otimes \frac{1}{\sqrt{2}}(\uparrow\downarrow - \downarrow\uparrow)]$ $+\frac{1}{\sqrt{6}}[(\{ds\}b) \otimes \frac{1}{\sqrt{6}}(\uparrow\downarrow\uparrow + \downarrow\uparrow\uparrow - 2\uparrow\uparrow\downarrow)][(u\bar{c}) \otimes \frac{1}{\sqrt{2}}(\uparrow\downarrow - \downarrow\uparrow)]$ $-\sqrt{\frac{2}{3}}[(\{ud\}b) \otimes \frac{1}{\sqrt{6}}(\uparrow\downarrow\uparrow + \downarrow\uparrow\uparrow - 2\uparrow\uparrow\downarrow)][(s\bar{c}) \otimes \frac{1}{\sqrt{2}}(\uparrow\downarrow - \downarrow\uparrow)]$
$P_{b\bar{c}}^4$	8_{2f}	$\frac{1}{\sqrt{2}}([us]b \otimes \frac{1}{\sqrt{2}}(\uparrow\downarrow\uparrow - \downarrow\uparrow\uparrow))(d\bar{c} \otimes \frac{1}{\sqrt{2}}(\uparrow\downarrow - \downarrow\uparrow))$ $+\frac{1}{\sqrt{2}}([ds]b \otimes \frac{1}{\sqrt{2}}(\uparrow\downarrow\uparrow - \downarrow\uparrow\uparrow))(u\bar{c} \otimes \frac{1}{\sqrt{2}}(\uparrow\downarrow - \downarrow\uparrow))$
$P_{b\bar{c}}^5$	8_{1f}	$\frac{1}{\sqrt{2}}[(\{us\}b) \otimes \frac{1}{\sqrt{6}}(\uparrow\downarrow\uparrow + \downarrow\uparrow\uparrow - 2\uparrow\uparrow\downarrow)][(d\bar{c}) \otimes \frac{1}{\sqrt{2}}(\uparrow\downarrow - \downarrow\uparrow)]$ $-\frac{1}{\sqrt{2}}[(\{ds\}b) \otimes \frac{1}{\sqrt{6}}(\uparrow\downarrow\uparrow + \downarrow\uparrow\uparrow - 2\uparrow\uparrow\downarrow)][(u\bar{c}) \otimes \frac{1}{\sqrt{2}}(\uparrow\downarrow - \downarrow\uparrow)]$
$P_{b\bar{c}}^5$	8_{2f}	$\frac{1}{\sqrt{6}}([us]b \otimes \frac{1}{\sqrt{2}}(\uparrow\downarrow\uparrow - \downarrow\uparrow\uparrow))(d\bar{c} \otimes \frac{1}{\sqrt{2}}(\uparrow\downarrow - \downarrow\uparrow))$ $-\frac{1}{\sqrt{6}}([ds]b \otimes \frac{1}{\sqrt{2}}(\uparrow\downarrow\uparrow - \downarrow\uparrow\uparrow))(u\bar{c} \otimes \frac{1}{\sqrt{2}}(\uparrow\downarrow - \downarrow\uparrow))$ $-\sqrt{\frac{2}{3}}([ud]b \otimes \frac{1}{\sqrt{2}}(\uparrow\downarrow\uparrow - \downarrow\uparrow\uparrow))(s\bar{c} \otimes \frac{1}{\sqrt{2}}(\uparrow\downarrow - \downarrow\uparrow))$
$P_{b\bar{c}}^6$	8_{1f}	$\sqrt{\frac{1}{3}}[(\{ds\}b) \otimes \frac{1}{\sqrt{6}}(\uparrow\downarrow\uparrow + \downarrow\uparrow\uparrow - 2\uparrow\uparrow\downarrow)][(d\bar{c}) \otimes \frac{1}{\sqrt{2}}(\uparrow\downarrow - \downarrow\uparrow)]$ $-\sqrt{\frac{2}{3}}[(\{dd\}b) \otimes \frac{1}{\sqrt{6}}(\uparrow\downarrow\uparrow + \downarrow\uparrow\uparrow - 2\uparrow\uparrow\downarrow)][(s\bar{c}) \otimes \frac{1}{\sqrt{2}}(\uparrow\downarrow - \downarrow\uparrow)]$
$P_{b\bar{c}}^6$	8_{2f}	$([ds]b \otimes \frac{1}{\sqrt{2}}(\uparrow\downarrow\uparrow - \downarrow\uparrow\uparrow))(d\bar{c} \otimes \frac{1}{\sqrt{2}}(\uparrow\downarrow - \downarrow\uparrow))$
$P_{b\bar{c}}^7$	8_{1f}	$\sqrt{\frac{1}{3}}[(\{us\}b) \otimes \frac{1}{\sqrt{6}}(\uparrow\downarrow\uparrow + \downarrow\uparrow\uparrow - 2\uparrow\uparrow\downarrow)][(s\bar{c}) \otimes \frac{1}{\sqrt{2}}(\uparrow\downarrow - \downarrow\uparrow)]$ $-\sqrt{\frac{2}{3}}[(\{ss\}b) \otimes \frac{1}{\sqrt{6}}(\uparrow\downarrow\uparrow + \downarrow\uparrow\uparrow - 2\uparrow\uparrow\downarrow)][(u\bar{c}) \otimes \frac{1}{\sqrt{2}}(\uparrow\downarrow - \downarrow\uparrow)]$
$P_{b\bar{c}}^7$	8_{2f}	$([us]b \otimes \frac{1}{\sqrt{2}}(\uparrow\downarrow\uparrow - \downarrow\uparrow\uparrow))(s\bar{c} \otimes \frac{1}{\sqrt{2}}(\uparrow\downarrow - \downarrow\uparrow))$
$P_{b\bar{c}}^8$	8_{1f}	$\sqrt{\frac{1}{3}}[(\{ds\}b) \otimes \frac{1}{\sqrt{6}}(\uparrow\downarrow\uparrow + \downarrow\uparrow\uparrow - 2\uparrow\uparrow\downarrow)][(s\bar{c}) \otimes \frac{1}{\sqrt{2}}(\uparrow\downarrow - \downarrow\uparrow)]$ $-\sqrt{\frac{2}{3}}[(\{ss\}b) \otimes \frac{1}{\sqrt{6}}(\uparrow\downarrow\uparrow + \downarrow\uparrow\uparrow - 2\uparrow\uparrow\downarrow)][(d\bar{c}) \otimes \frac{1}{\sqrt{2}}(\uparrow\downarrow - \downarrow\uparrow)]$
$P_{b\bar{c}}^8$	8_{2f}	$([ds]b \otimes \frac{1}{\sqrt{2}}(\uparrow\downarrow\uparrow - \downarrow\uparrow\uparrow))(s\bar{c} \otimes \frac{1}{\sqrt{2}}(\uparrow\downarrow - \downarrow\uparrow))$

bulk of near-threshold $bc\bar{q}qq$ and $\bar{b}cqqq$ candidates in octet configurations. Third, restricting the calculation to the two octets allows a clean and physically transparent comparison between the symmetric and antisymmetric light-diquark sectors, which is one of the central themes of this paper. A complete treatment of the 10_f (built from $6_f \otimes 3_f$) and 1_f (built from $\bar{3}_f \otimes 3_f$) representations is straightforward within the same formalism and is left for future investigation.

The spin structure follows from the quantum numbers of the constituents. Baryons built from a symmetric light-

TABLE II. Fully explicit spin-flavor wave functions of the $c\bar{b}$ molecular pentaquark octet. The arrows denote quark spin projections. Here $\{q_1 q_2\}$ and $[q_1 q_2]$ denote symmetric and antisymmetric light-diquark flavor combinations, respectively.

State	Representation	$\psi_{\text{flavor}} \otimes \chi_{\text{spin}}$
$P_{c\bar{b}}^1$	8_{1f}	$-\sqrt{\frac{1}{3}}[(\{ud\}c) \otimes \frac{1}{\sqrt{6}}(\uparrow\downarrow\uparrow + \downarrow\uparrow\uparrow - 2\uparrow\uparrow\downarrow)][(u\bar{b}) \otimes \frac{1}{\sqrt{2}}(\uparrow\downarrow - \downarrow\uparrow)]$ $+\sqrt{\frac{2}{3}}[(\{uu\}c) \otimes \frac{1}{\sqrt{6}}(\uparrow\downarrow\uparrow + \downarrow\uparrow\uparrow - 2\uparrow\uparrow\downarrow)][(d\bar{b}) \otimes \frac{1}{\sqrt{2}}(\uparrow\downarrow - \downarrow\uparrow)]$
$P_{c\bar{b}}^1$	8_{2f}	$([ud]c \otimes \frac{1}{\sqrt{2}}(\uparrow\downarrow\uparrow - \downarrow\uparrow\uparrow))(u\bar{b} \otimes \frac{1}{\sqrt{2}}(\uparrow\downarrow - \downarrow\uparrow))$
$P_{c\bar{b}}^2$	8_{1f}	$\sqrt{\frac{1}{3}}[(\{ud\}c) \otimes \frac{1}{\sqrt{6}}(\uparrow\downarrow\uparrow + \downarrow\uparrow\uparrow - 2\uparrow\uparrow\downarrow)][(d\bar{b}) \otimes \frac{1}{\sqrt{2}}(\uparrow\downarrow - \downarrow\uparrow)]$ $-\sqrt{\frac{2}{3}}[(\{dd\}c) \otimes \frac{1}{\sqrt{6}}(\uparrow\downarrow\uparrow + \downarrow\uparrow\uparrow - 2\uparrow\uparrow\downarrow)][(u\bar{b}) \otimes \frac{1}{\sqrt{2}}(\uparrow\downarrow - \downarrow\uparrow)]$
$P_{c\bar{b}}^2$	8_{2f}	$([ud]c \otimes \frac{1}{\sqrt{2}}(\uparrow\downarrow\uparrow - \downarrow\uparrow\uparrow))(d\bar{b} \otimes \frac{1}{\sqrt{2}}(\uparrow\downarrow - \downarrow\uparrow))$
$P_{c\bar{b}}^3$	8_{1f}	$\sqrt{\frac{1}{3}}[(\{us\}c) \otimes \frac{1}{\sqrt{6}}(\uparrow\downarrow\uparrow + \downarrow\uparrow\uparrow - 2\uparrow\uparrow\downarrow)][(u\bar{b}) \otimes \frac{1}{\sqrt{2}}(\uparrow\downarrow - \downarrow\uparrow)]$ $-\sqrt{\frac{2}{3}}[(\{uu\}c) \otimes \frac{1}{\sqrt{6}}(\uparrow\downarrow\uparrow + \downarrow\uparrow\uparrow - 2\uparrow\uparrow\downarrow)][(s\bar{b}) \otimes \frac{1}{\sqrt{2}}(\uparrow\downarrow - \downarrow\uparrow)]$
$P_{c\bar{b}}^3$	8_{2f}	$([us]c \otimes \frac{1}{\sqrt{2}}(\uparrow\downarrow\uparrow - \downarrow\uparrow\uparrow))(u\bar{b} \otimes \frac{1}{\sqrt{2}}(\uparrow\downarrow - \downarrow\uparrow))$
$P_{c\bar{b}}^4$	8_{1f}	$\frac{1}{\sqrt{6}}[(\{us\}c) \otimes \frac{1}{\sqrt{6}}(\uparrow\downarrow\uparrow + \downarrow\uparrow\uparrow - 2\uparrow\uparrow\downarrow)][(d\bar{b}) \otimes \frac{1}{\sqrt{2}}(\uparrow\downarrow - \downarrow\uparrow)]$ $+\frac{1}{\sqrt{6}}[(\{ds\}c) \otimes \frac{1}{\sqrt{6}}(\uparrow\downarrow\uparrow + \downarrow\uparrow\uparrow - 2\uparrow\uparrow\downarrow)][(u\bar{b}) \otimes \frac{1}{\sqrt{2}}(\uparrow\downarrow - \downarrow\uparrow)]$ $-\sqrt{\frac{2}{3}}[(\{ud\}c) \otimes \frac{1}{\sqrt{6}}(\uparrow\downarrow\uparrow + \downarrow\uparrow\uparrow - 2\uparrow\uparrow\downarrow)][(s\bar{b}) \otimes \frac{1}{\sqrt{2}}(\uparrow\downarrow - \downarrow\uparrow)]$
$P_{c\bar{b}}^4$	8_{2f}	$\frac{1}{\sqrt{2}}([us]c \otimes \frac{1}{\sqrt{2}}(\uparrow\downarrow\uparrow - \downarrow\uparrow\uparrow))(d\bar{b} \otimes \frac{1}{\sqrt{2}}(\uparrow\downarrow - \downarrow\uparrow))$ $+\frac{1}{\sqrt{2}}([ds]c \otimes \frac{1}{\sqrt{2}}(\uparrow\downarrow\uparrow - \downarrow\uparrow\uparrow))(u\bar{b} \otimes \frac{1}{\sqrt{2}}(\uparrow\downarrow - \downarrow\uparrow))$
$P_{c\bar{b}}^5$	8_{1f}	$\frac{1}{\sqrt{2}}[(\{us\}c) \otimes \frac{1}{\sqrt{6}}(\uparrow\downarrow\uparrow + \downarrow\uparrow\uparrow - 2\uparrow\uparrow\downarrow)][(d\bar{b}) \otimes \frac{1}{\sqrt{2}}(\uparrow\downarrow - \downarrow\uparrow)]$ $-\frac{1}{\sqrt{2}}[(\{ds\}c) \otimes \frac{1}{\sqrt{6}}(\uparrow\downarrow\uparrow + \downarrow\uparrow\uparrow - 2\uparrow\uparrow\downarrow)][(u\bar{b}) \otimes \frac{1}{\sqrt{2}}(\uparrow\downarrow - \downarrow\uparrow)]$
$P_{c\bar{b}}^5$	8_{2f}	$\frac{1}{\sqrt{6}}([us]c \otimes \frac{1}{\sqrt{2}}(\uparrow\downarrow\uparrow - \downarrow\uparrow\uparrow))(d\bar{b} \otimes \frac{1}{\sqrt{2}}(\uparrow\downarrow - \downarrow\uparrow))$ $-\frac{1}{\sqrt{6}}([ds]c \otimes \frac{1}{\sqrt{2}}(\uparrow\downarrow\uparrow - \downarrow\uparrow\uparrow))(u\bar{b} \otimes \frac{1}{\sqrt{2}}(\uparrow\downarrow - \downarrow\uparrow))$ $-\sqrt{\frac{2}{3}}([ud]c \otimes \frac{1}{\sqrt{2}}(\uparrow\downarrow\uparrow - \downarrow\uparrow\uparrow))(s\bar{b} \otimes \frac{1}{\sqrt{2}}(\uparrow\downarrow - \downarrow\uparrow))$
$P_{c\bar{b}}^6$	8_{1f}	$\sqrt{\frac{1}{3}}[(\{ds\}c) \otimes \frac{1}{\sqrt{6}}(\uparrow\downarrow\uparrow + \downarrow\uparrow\uparrow - 2\uparrow\uparrow\downarrow)][(d\bar{b}) \otimes \frac{1}{\sqrt{2}}(\uparrow\downarrow - \downarrow\uparrow)]$ $-\sqrt{\frac{2}{3}}[(\{dd\}c) \otimes \frac{1}{\sqrt{6}}(\uparrow\downarrow\uparrow + \downarrow\uparrow\uparrow - 2\uparrow\uparrow\downarrow)][(s\bar{b}) \otimes \frac{1}{\sqrt{2}}(\uparrow\downarrow - \downarrow\uparrow)]$
$P_{c\bar{b}}^6$	8_{2f}	$([ds]c \otimes \frac{1}{\sqrt{2}}(\uparrow\downarrow\uparrow - \downarrow\uparrow\uparrow))(d\bar{b} \otimes \frac{1}{\sqrt{2}}(\uparrow\downarrow - \downarrow\uparrow))$
$P_{c\bar{b}}^7$	8_{1f}	$\sqrt{\frac{1}{3}}[(\{us\}c) \otimes \frac{1}{\sqrt{6}}(\uparrow\downarrow\uparrow + \downarrow\uparrow\uparrow - 2\uparrow\uparrow\downarrow)][(s\bar{b}) \otimes \frac{1}{\sqrt{2}}(\uparrow\downarrow - \downarrow\uparrow)]$ $-\sqrt{\frac{2}{3}}[(\{ss\}c) \otimes \frac{1}{\sqrt{6}}(\uparrow\downarrow\uparrow + \downarrow\uparrow\uparrow - 2\uparrow\uparrow\downarrow)][(u\bar{b}) \otimes \frac{1}{\sqrt{2}}(\uparrow\downarrow - \downarrow\uparrow)]$
$P_{c\bar{b}}^7$	8_{2f}	$([us]c \otimes \frac{1}{\sqrt{2}}(\uparrow\downarrow\uparrow - \downarrow\uparrow\uparrow))(s\bar{b} \otimes \frac{1}{\sqrt{2}}(\uparrow\downarrow - \downarrow\uparrow))$
$P_{c\bar{b}}^8$	8_{1f}	$\sqrt{\frac{1}{3}}[(\{ds\}c) \otimes \frac{1}{\sqrt{6}}(\uparrow\downarrow\uparrow + \downarrow\uparrow\uparrow - 2\uparrow\uparrow\downarrow)][(s\bar{b}) \otimes \frac{1}{\sqrt{2}}(\uparrow\downarrow - \downarrow\uparrow)]$ $-\sqrt{\frac{2}{3}}[(\{ss\}c) \otimes \frac{1}{\sqrt{6}}(\uparrow\downarrow\uparrow + \downarrow\uparrow\uparrow - 2\uparrow\uparrow\downarrow)][(d\bar{b}) \otimes \frac{1}{\sqrt{2}}(\uparrow\downarrow - \downarrow\uparrow)]$
$P_{c\bar{b}}^8$	8_{2f}	$([ds]c \otimes \frac{1}{\sqrt{2}}(\uparrow\downarrow\uparrow - \downarrow\uparrow\uparrow))(s\bar{b} \otimes \frac{1}{\sqrt{2}}(\uparrow\downarrow - \downarrow\uparrow))$

diquark configuration exist with both $J_B^{P_B} = \frac{1}{2}^+$ and $\frac{3}{2}^+$, whereas those built from an antisymmetric light-diquark configuration are restricted to $J_B^{P_B} = \frac{1}{2}^+$. The heavy-light mesons ($q\bar{Q}'$) appear with spin-parity $J_M^{P_M} = 0^-$ and 1^- . For S-wave molecules, the total spin-parity is obtained from

$$J = S_B \oplus S_M, \quad P = P_B P_M, \quad (9)$$

leading to the lowest configurations

$$J^P = \frac{1}{2}^- (\frac{1}{2}^+ \otimes 0^-), \quad J^P = \frac{1}{2}^- (\frac{1}{2}^+ \otimes 1^-), \quad J^P = \frac{3}{2}^- (\frac{1}{2}^+ \otimes 1^-). \quad (10)$$

The $SU(3)_f$ spin-flavor wave functions of the $b\bar{c}$ and $c\bar{b}$ pentaquark octets are listed in Tables I and II, both at the hadronic level (baryon \otimes meson) and at the quark level (in terms of $\{q_1q_2\}$ and $[q_1q_2]$). The 8_{1f} representation comes from $6_f \otimes 3_f$ (symmetric diquarks) and the 8_{2f} from $\bar{3}_f \otimes 3_f$ (antisymmetric diquarks); the orthogonality of the octet states follows from the underlying Clebsch–Gordan algebra.

The molecular assignment adopted here is supported by dynamical studies: coupled-channel calculations in the local hidden-gauge approach generate bound states near the relevant baryon–meson thresholds for the $\bar{c}bqqq$ and $b\bar{c}qqq$ systems [29], and the extended hidden-gauge analysis of Ref. [30] identifies fourteen S-wave molecular candidates — including bottom–charm states — close to the corresponding thresholds. The near-threshold character of these states is the standard criterion for a molecular interpretation, and the present work takes those results as motivation for computing their electromagnetic properties. Earlier predictions of heavy-baryon–heavy-meson molecules within the one-boson-exchange model are given in Ref. [32].

III. MAGNETIC MOMENTS

We now compute the magnetic moments of the $b\bar{c}$ and $c\bar{b}$ molecular pentaquarks in the constituent quark model. The magnetic moment is in general a vector observable, $\hat{\mu}$; following standard convention, the scalar quantity referred to as “the magnetic moment” μ of a hadron with total angular momentum J is defined as

$$\mu \equiv \langle J, M_J = J | \hat{\mu}_z | J, M_J = J \rangle, \quad \hat{\mu}_z \equiv \hat{\mu} \cdot \hat{e}_z. \quad (11)$$

Throughout this section all operator equations are written for the vector $\hat{\mu}$; the numerical entries of Tables III and IV correspond to the scalar projection μ .

The hadronic magnetic moment receives intrinsic-spin and orbital contributions, $\hat{\mu} = \hat{\mu}_{\text{spin}} + \hat{\mu}_{\text{orbital}}$. For the S-wave molecules considered here the relative orbital angular momentum vanishes ($L = 0$), so only the spin contribution remains, with

$$\hat{\mu}_{\text{spin}} = \sum_i \frac{Q_i}{2M_i} \hat{\sigma}_i, \quad (12)$$

where Q_i , M_i , $\hat{\sigma}_i$ are the electric charge (in units of e), constituent mass, and Pauli spin vector of the i -th quark. Projecting onto the z -axis gives the elementary single-quark matrix elements $\langle q \uparrow | \hat{\mu}_z | q \uparrow \rangle = +Q_q/(2M_q)$ and $\langle q \downarrow | \hat{\mu}_z | q \downarrow \rangle = -Q_q/(2M_q)$.

In the molecular picture, an S-wave pentaquark is a coherent superposition of baryon–meson channels, and its magnetic-moment operator decomposes as

$$\hat{\mu} = \hat{\mu}_B + \hat{\mu}_M, \quad (13)$$

where $\hat{\mu}_B$ and $\hat{\mu}_M$ are the (vector) operators of the baryon and meson components. This additive form follows directly from the factorization established below Eq. (2): since $\hat{\mu}$ is local at the quark level and the molecular spatial wave function is normalized, the diagonal pentaquark moment equals the sum of the constituent-hadron moments with no inter-hadron form-factor suppression.

To illustrate the quark-model calculation, consider the antisymmetric bottom baryon $\Lambda_b^0 \equiv [ud]b$ with $J^P = \frac{1}{2}^+$. Its spin-flavor wave function for $S_z = +\frac{1}{2}$ is

$$|\Lambda_b^0, S_z = +\frac{1}{2}\rangle = \frac{1}{\sqrt{2}}(ud - du)b \otimes \frac{1}{\sqrt{2}}(\uparrow\downarrow - \downarrow\uparrow). \quad (14)$$

Applying $\hat{\mu}_z = \sum_i (Q_i/2M_i)\sigma_z^{(i)}$ and evaluating the spin matrix elements gives the compact result $\mu_{\Lambda_b^0} = \mu_b$, where $\mu_q \equiv Q_q/(2M_q)$: the two light quarks in the antisymmetric $[ud]$ diquark couple to spin zero, so the moment is carried entirely by the heavy b quark.

As a concrete illustration, consider the neutral open bottom–charm molecular pentaquark belonging to the 8_{1f} representation. Its quark-level flavor wave function reads

$$P_{b\bar{c}}^2(8_{1f}) = \sqrt{\frac{1}{3}}\{ud\}b d\bar{c} - \sqrt{\frac{2}{3}}\{dd\}b u\bar{c}. \quad (15)$$

For the S-wave configuration with $J^P = \frac{1}{2}^-(\frac{1}{2}^+ \otimes 0^-)$, the meson carries zero spin and the total angular momentum is provided by the baryon; the explicit spin-flavor state with $M = +\frac{1}{2}$ is given in Table I. Evaluating $\hat{\mu}_z = \sum_i \hat{\mu}_i$ on this state yields

$$\mu[P_{b\bar{c}}^2(8_{1f})] = \frac{4}{3}\mu_d - \frac{1}{3}\mu_b + \frac{1}{3}\mu_d + \frac{2}{3}\mu_u + \mu_{\bar{c}}, \quad (16)$$

in agreement with the expression used in the numerical analysis; substituting the constituent-quark moments yields the prediction listed in Table III.

IV. RESULTS AND DISCUSSION

We use the constituent quark masses $m_u = m_d = 361.8$ MeV, $m_s = 540.4$ MeV, $m_c = 1724.8$ MeV, and $m_b = 5052.9$ MeV [28]. The molecular masses of the open bottom-charm pentaquarks are not computed here; they are taken from Refs. [29, 30], which predict the corresponding states to lie close to the relevant baryon-meson thresholds. For convenience, Tables III and IV list, in addition to the magnetic moments, the dominant baryon-meson channels of each $P_{b\bar{c}}^k$ and $P_{c\bar{b}}^k$ and the corresponding thresholds from PDG averages [31]; the predicted molecular masses lie typically 10–50 MeV below these thresholds. Thus, for example, $P_{b\bar{c}}^1(8_{2f})$ should be sought in $\Lambda_b \bar{D}$ near 7484 MeV and $P_{c\bar{b}}^1(8_{2f})$ in $\Lambda_c B$ near 7566 MeV. The magnetic moments of the $b\bar{c}$ and $c\bar{b}$ octets exhibit a rich and systematic structure that links the electromagnetic properties directly to the underlying quark dynamics, spin coupling, and heavy-quark ordering, as discussed in the subsections below.

A. Pseudoscalar channel: $\frac{1}{2}^+ \otimes 0^-$, $J^P = \frac{1}{2}^-$

The $\frac{1}{2}^+ \otimes 0^-$ configuration demonstrates a fundamental dichotomy between the two flavor representations. In the 8_{2f} representation, a near-perfect universality is observed. Every $b\bar{c}$ state from $P_{b\bar{c}}^1$ through $P_{b\bar{c}}^8$ possesses an identical magnetic moment of $\mu = -0.062 \mu_N$, and every $c\bar{b}$ state shares the value $\mu = +0.362 \mu_N$. This constancy is a direct and powerful consequence of the antisymmetric nature of the light-diquark in the 8_{2f} wave function. In this configuration, the two light quarks are forced into a spin-singlet state, effectively silencing their contribution to the magnetic moment. Furthermore, the pseudoscalar meson partner carries zero spin. Consequently, the magnetic moment of the entire molecular system is almost entirely dictated by the single heavy quark (or antiquark) residing within the baryon component. The sign reversal between the $b\bar{c}$ and $c\bar{b}$ families encodes the change in the dominant heavy constituent electric charge, while the magnitude difference reflects the inverse mass scaling: the charm quark larger magnetic moment due to its lower mass dominates in the $c\bar{b}$ case. This provides an exceptionally clean electromagnetic signature for any state belonging to the 8_{2f} molecular multiplet, making these predictions particularly robust and testable.

The behavior of the same $\frac{1}{2}^+ \otimes 0^-$ configurations in the 8_{1f} representation is markedly different. Here the light diquark is in a symmetric spin-triplet configuration, allowing the light quarks to contribute actively to the total magnetic moment. As a result, the predicted values span a broad range including both positive and negative magnetic moments that depend sensitively on the flavor composition of each state. For the $b\bar{c}$ sector, the values vary from large positive $\mu(P_{b\bar{c}}^1) = +1.749 \mu_N$ and $\mu(P_{b\bar{c}}^3) = +1.812 \mu_N$, to moderate positive $\mu(P_{b\bar{c}}^4) = +0.372 \mu_N$, and to negative values $\mu(P_{b\bar{c}}^2) = -0.555 \mu_N$, $\mu(P_{b\bar{c}}^6) = -1.068 \mu_N$, $\mu(P_{b\bar{c}}^7) = -0.238 \mu_N$, and $\mu(P_{b\bar{c}}^8) = -0.814 \mu_N$. The state $P_{b\bar{c}}^5$ yields a comparatively small value $\mu(P_{b\bar{c}}^5) = -0.077 \mu_N$, reflecting a partial cancellation among contributions from different quark components. A similar pattern appears in the $c\bar{b}$ sector: $\mu(P_{c\bar{b}}^1) = +1.607 \mu_N$, $\mu(P_{c\bar{b}}^3) = +1.671 \mu_N$, $\mu(P_{c\bar{b}}^4) = +0.231 \mu_N$, $\mu(P_{c\bar{b}}^2) = -0.697 \mu_N$, $\mu(P_{c\bar{b}}^6) = -1.210 \mu_N$, $\mu(P_{c\bar{b}}^7) = -0.380 \mu_N$, $\mu(P_{c\bar{b}}^8) = -0.956 \mu_N$, and $\mu(P_{c\bar{b}}^5) = -0.218 \mu_N$. This wide spread of values originates from the interplay among the magnetic moments of the u , d , and s quarks in the symmetric light-diquark configuration together with the heavy quark contributions. Since $\mu_q = Q_q/(2m_q)$, the different masses and charges of the b and c quarks directly produce quantitative differences between the $b\bar{c}$ and $c\bar{b}$ sectors, and the 8_{1f} representation consequently displays a much richer structure than the nearly universal pattern of the 8_{2f} case.

B. Vector channel: $\frac{1}{2}^+ \otimes 1^-$, $J^P = \frac{1}{2}^-$

The introduction of a vector meson through the $\frac{1}{2}^+ \otimes 1^-$ configuration significantly enriches the observed patterns and highlights the critical role of spin coupling. The magnetic moments show substantial deviations from their

pseudoscalar counterparts, often involving sign changes that reflect destructive interference between the baryon and vector-meson spin contributions.

A representative example is the state $P_{b\bar{c}}^1$. Its magnetic moment changes from $\mu(P_{b\bar{c}}^1) = +1.749 \mu_N$ in the $\frac{1}{2}^+ \otimes 0^-$ channel to $\mu(P_{b\bar{c}}^1) = -0.824 \mu_N$ in the $\frac{1}{2}^+ \otimes 1^-$ channel within the 8_{1f} representation. In contrast, in the 8_{2f} representation the same configuration yields $\mu(P_{b\bar{c}}^1) = +0.931 \mu_N$. This demonstrates that the underlying flavor symmetry can qualitatively alter, and even reverse, the interference pattern that governs the magnetic moment. Such large shifts and sign reversals are a generic feature across both the $b\bar{c}$ and $c\bar{b}$ octets.

A comparison of corresponding states further illustrates the interplay between flavor structure and spin coupling. For the pair $P_{b\bar{c}}^2$ and $P_{c\bar{b}}^2$, one finds $\mu(P_{b\bar{c}}^2) = +0.519 \mu_N$ and $\mu(P_{c\bar{b}}^2) = +0.273 \mu_N$ for the $J = \frac{1}{2}$ states in the 8_{1f} representation, indicating similar constructive spin alignment. However, their $J = \frac{3}{2}$ moments differ noticeably: $\mu(P_{b\bar{c}}^3) = -0.054 \mu_N$, while $\mu(P_{c\bar{b}}^3) = -0.635 \mu_N$, showing that the heavy-quark content significantly affects higher-spin configurations.

The pair $P_{b\bar{c}}^3$ and $P_{c\bar{b}}^3$ exhibits a consistent pattern across both spin sectors. For $J = \frac{1}{2}$, the magnetic moments are negative, $\mu(P_{b\bar{c}}^3) = -0.719 \mu_N$ and $\mu(P_{c\bar{b}}^3) = -0.965 \mu_N$, while for $J = \frac{3}{2}$ they become positive, $\mu(P_{b\bar{c}}^6) = +1.640 \mu_N$ and $\mu(P_{c\bar{b}}^6) = +1.671 \mu_N$. This behavior indicates a common spin-coupling mechanism in which the higher-spin configuration favors constructive alignment of the constituent magnetic moments despite the interchange of heavy quarks. The states $P_{b\bar{c}}^6$ and $P_{c\bar{b}}^6$ are distinguished by their large magnitudes across different configurations, reflecting a flavor structure that enhances additive contributions. In particular, the $J = \frac{3}{2}$ state of $P_{b\bar{c}}^6$ reaches $\mu(P_{b\bar{c}}^6) = -2.104 \mu_N$ in the 8_{1f} representation, one of the largest values in the spectrum.

C. Vector channel: $\frac{1}{2}^+ \otimes 1^-$, $J^P = \frac{3}{2}^-$

The $J^P = \frac{3}{2}^-$ states, originating from maximal spin alignment in the $\frac{1}{2}^+ \otimes 1^-$ coupling, systematically exhibit the largest magnetic moments in magnitude across both $SU(3)_f$ representations and both heavy-quark sectors. This enhancement follows from the coherent addition of spin contributions from the baryon and the vector meson.

The effect is particularly pronounced in the $c\bar{b}$ sector, where the charm quark carries a comparatively larger intrinsic magnetic moment. A representative example is the state $P_{c\bar{b}}^1$, for which

$$\mu(P_{c\bar{b}}^1) = +2.533 \mu_N \quad (17)$$

in the 8_{1f} representation for $J = \frac{3}{2}$, making it one of the largest magnetic moments in the spectrum.

This behavior is generic, indicating that the $J = \frac{3}{2}$ states are the most electromagnetically enhanced configurations and therefore the most favorable candidates for observation in electromagnetic processes. The dependence on the flavor representation remains significant. For instance, the state $P_{c\bar{b}}^6$ shows a pronounced variation between the two octets:

$$\mu(P_{c\bar{b}}^6) = -0.957 \mu_N \quad (8_{1f}), \quad (18)$$

$$\mu(P_{c\bar{b}}^6) = +2.153 \mu_N \quad (8_{2f}). \quad (19)$$

The large magnitude difference and the sign reversal clearly demonstrate the sensitivity of magnetic moments to the underlying flavor structure. Such behavior provides a powerful diagnostic tool for distinguishing between the 8_{1f} and 8_{2f} assignments of experimentally observed states.

D. Theoretical implications

Several implications follow from these results. First, the systematic gap between the 8_{1f} and 8_{2f} predictions establishes the magnetic moment as a useful discriminator of the internal flavor structure of molecular pentaquarks. Second, the differences between the $b\bar{c}$ and $c\bar{b}$ families across all spin-parity configurations constitute explicit evidence of heavy-quark flavor symmetry breaking in electromagnetic observables: since $\mu \propto Q/m$, interchanging the roles of the b and c quarks between the baryon and meson modifies the relative quark-sector contributions in a way not captured by simple symmetry arguments. The sign change of the universal 8_{2f} pseudoscalar moment between families — from $\mu \approx -0.062 \mu_N$ for $b\bar{c}$ to $\mu \approx +0.362 \mu_N$ for $c\bar{b}$ — is the cleanest manifestation of this breaking. Third, the sizable splitting between $J = 1/2$ and $J = 3/2$ moments arising from the same hadronic configuration provides a

potential indicator for spin determination, complementary to angular-distribution analyses [33–37]. Fourth, the near-vanishing $\mu(P_{b\bar{c}}^5) = -0.077 \mu_N$ in the 8_{1f} pseudoscalar channel reflects a fine balance between light- and heavy-quark contributions within the adopted mass scheme.

Direct measurements of static moments for short-lived pentaquarks are currently beyond reach, but indirect access is possible through radiative decay widths, proportional to the cube of the photon energy and the square of the transition magnetic moment [38]. The diagonal moments tabulated here are insufficient for that purpose: radiative widths require off-diagonal matrix elements $\langle \Psi' | \hat{\mu}_z | \Psi \rangle$ between states of different spin–parity configuration, which explicitly involve the spatial overlap $\langle \eta'_{\text{space}} | \eta_{\text{space}} \rangle$ between the initial and final molecules. In the loosely-bound limit this overlap acts as a form-factor-like suppression sensitive to the binding dynamics; its quantitative treatment, requiring an explicit spatial wave function, is left for future work. Production asymmetries in polarized collisions at LHCb, Belle II and the Electron–Ion Collider may provide further indirect probes, and the predictions tabulated here serve as benchmarks for such future analyses.

TABLE III. Magnetic moments of the $b\bar{c}$ octet molecular pentaquark family states, in units of the nuclear magneton μ_N . The third column lists the dominant baryon–meson channels for each representation (full spin–flavor combinations are given in Table I). The fourth column gives the approximate thresholds (sums of constituent masses from PDG averages [31]) for the pseudoscalar (PS) and vector (V) meson channels.

State	$J_B^{P_b} \otimes J_M^{P_m}$	Channels [$8_{2f} / 8_{1f}$]	Threshold (MeV) PS / V	$I(J^P)$	$\mu(8_{1f})$	$\mu(8_{2f})$
$P_{b\bar{c}}^1$	$\frac{1}{2}^+ \otimes 0^-$ $\frac{1}{2}^+ \otimes 1^-$	$\Lambda_b \bar{D} / \Sigma_b \bar{D}$	7484 / 7676	$\frac{1}{2}(\frac{1}{2}^-)$	1.749	−0.062
			7627 / 7820	$\frac{1}{2}(\frac{1}{2}^-)$	−0.824	0.931
				$\frac{1}{2}(\frac{3}{2}^-)$	1.386	1.304
$P_{b\bar{c}}^2$	$\frac{1}{2}^+ \otimes 0^-$ $\frac{1}{2}^+ \otimes 1^-$	$\Lambda_b D / \Sigma_b D$	7489 / 7681	$\frac{1}{2}(\frac{1}{2}^-)$	−0.555	−0.062
			7630 / 7822	$\frac{1}{2}(\frac{1}{2}^-)$	0.519	−0.797
				$\frac{1}{2}(\frac{3}{2}^-)$	−0.054	−1.289
$P_{b\bar{c}}^3$	$\frac{1}{2}^+ \otimes 0^-$ $\frac{1}{2}^+ \otimes 1^-$	$\Xi_b \bar{D} / \Xi_b' \bar{D}, \Sigma_b D_s$	7657 / 7779	$1(\frac{1}{2}^-)$	1.812	−0.062
			7799 / 7923	$1(\frac{1}{2}^-)$	−0.719	0.931
				$1(\frac{3}{2}^-)$	1.640	1.304
$P_{b\bar{c}}^4$	$\frac{1}{2}^+ \otimes 0^-$ $\frac{1}{2}^+ \otimes 1^-$	$\Xi_b D, \Xi_b \bar{D} / \Xi_b' \bar{D}, \Sigma_b D_s$	7662 / 7784	$1(\frac{1}{2}^-)$	0.372	−0.062
			7803 / 7925	$1(\frac{1}{2}^-)$	−0.527	0.670
				$1(\frac{3}{2}^-)$	−0.232	0.008
$P_{b\bar{c}}^5$	$\frac{1}{2}^+ \otimes 0^-$ $\frac{1}{2}^+ \otimes 1^-$	$\Lambda_b D_s, \Xi_b D / \Xi_b' \bar{D}, \Sigma_b D_s$	7588 / 7779	$0(\frac{1}{2}^-)$	−0.077	−0.062
			7731 / 7923	$0(\frac{1}{2}^-)$	0.072	−0.382
				$0(\frac{3}{2}^-)$	−0.007	−0.666
$P_{b\bar{c}}^6$	$\frac{1}{2}^+ \otimes 0^-$ $\frac{1}{2}^+ \otimes 1^-$	$\Xi_b D / \Xi_b' D, \Sigma_b D_s$	7667 / 7784	$1(\frac{1}{2}^-)$	−1.068	−0.062
			7807 / 7925	$1(\frac{1}{2}^-)$	−0.335	−0.797
				$1(\frac{3}{2}^-)$	−2.104	−1.289
$P_{b\bar{c}}^7$	$\frac{1}{2}^+ \otimes 0^-$ $\frac{1}{2}^+ \otimes 1^-$	$\Xi_b D_s / \Xi_b' D_s, \Omega_b \bar{D}$	7760 / 7903	$\frac{1}{2}(\frac{1}{2}^-)$	−0.238	−0.062
			7904 / 8049	$\frac{1}{2}(\frac{1}{2}^-)$	0.477	−0.607
				$\frac{1}{2}(\frac{3}{2}^-)$	0.359	−1.003
$P_{b\bar{c}}^8$	$\frac{1}{2}^+ \otimes 0^-$ $\frac{1}{2}^+ \otimes 1^-$	$\Xi_b D_s / \Xi_b' D_s, \Omega_b D$	7765 / 7903	$\frac{1}{2}(\frac{1}{2}^-)$	−0.814	−0.062
			7907 / 8049	$\frac{1}{2}(\frac{1}{2}^-)$	−0.483	−0.607
				$\frac{1}{2}(\frac{3}{2}^-)$	−1.946	−1.003

Figure 1 summarizes the magnetic moments in both representations and visually confirms the hierarchies discussed above: the near-universal values for the 8_{2f} pseudoscalar states, the broad dispersion in the 8_{1f} pseudoscalar states, the substantial shifts and sign changes upon introducing vector mesons, and the consistently largest magnitudes for the $J^P = \frac{3}{2}^-$ configurations.

V. FINAL REMARKS

We have computed the magnetic moments of the open bottom–charm and charm–antibottom molecular pentaquark octets in the constituent quark model, using explicitly constructed spin–flavor wave functions of the two $SU(3)_f$

TABLE IV. Magnetic moments of the $c\bar{b}$ octet molecular pentaquark family states, in units of the nuclear magneton μ_N . The third column lists the dominant baryon–meson channels for each representation (full spin–flavor combinations are given in Table II). The fourth column gives the approximate thresholds (sums of constituent masses from PDG averages [31]) for the pseudoscalar (PS) and vector (V) meson channels.

State	$J_B^{P_b} \otimes J_M^{P_m}$	Channels [$8_{2f} / 8_{1f}$]	Threshold (MeV) PS / V	$I(J^P)$	$\mu(8_{1f})$	$\mu(8_{2f})$
P_{cb}^1	$\frac{1}{2}^+ \otimes 0^-$ $\frac{1}{2}^+ \otimes 1^-$	$\Lambda_c B / \Sigma_c B$	7566 / 7732	$\frac{1}{2}(\frac{1}{2}^-)$	1.607	0.362
			7611 / 7777	$\frac{1}{2}(\frac{1}{2}^-)$	0.081	−0.656
				$\frac{1}{2}(\frac{3}{2}^-)$	2.533	−0.440
P_{cb}^2	$\frac{1}{2}^+ \otimes 0^-$ $\frac{1}{2}^+ \otimes 1^-$	$\Lambda_c B / \Sigma_c B$	7566 / 7732	$\frac{1}{2}(\frac{1}{2}^-)$	−0.697	0.362
			7611 / 7777	$\frac{1}{2}(\frac{1}{2}^-)$	0.273	1.073
				$\frac{1}{2}(\frac{3}{2}^-)$	−0.635	2.153
P_{cb}^3	$\frac{1}{2}^+ \otimes 0^-$ $\frac{1}{2}^+ \otimes 1^-$	$\Xi_c B / \Xi'_c B, \Sigma_c B_s$	7747 / 7857	$1(\frac{1}{2}^-)$	1.671	0.362
			7792 / 7903	$1(\frac{1}{2}^-)$	−0.965	−0.656
				$1(\frac{3}{2}^-)$	1.060	−0.440
P_{cb}^4	$\frac{1}{2}^+ \otimes 0^-$ $\frac{1}{2}^+ \otimes 1^-$	$\Xi_c B / \Xi'_c B, \Sigma_c B_s$	7747 / 7857	$1(\frac{1}{2}^-)$	0.231	0.362
			7792 / 7903	$1(\frac{1}{2}^-)$	−0.197	0.208
				$1(\frac{3}{2}^-)$	0.051	0.856
P_{cb}^5	$\frac{1}{2}^+ \otimes 0^-$ $\frac{1}{2}^+ \otimes 1^-$	$\Lambda_c B_s, \Xi_c B / \Xi'_c B, \Sigma_c B_s$	7653 / 7857	$0(\frac{1}{2}^-)$	−0.218	0.362
			7702 / 7903	$0(\frac{1}{2}^-)$	0.402	−0.241
				$0(\frac{3}{2}^-)$	0.275	0.183
P_{cb}^6	$\frac{1}{2}^+ \otimes 0^-$ $\frac{1}{2}^+ \otimes 1^-$	$\Xi_c B / \Xi'_c B, \Sigma_c B_s$	7750 / 7858	$1(\frac{1}{2}^-)$	−1.210	0.362
			7795 / 7903	$1(\frac{1}{2}^-)$	0.571	1.073
				$1(\frac{3}{2}^-)$	−0.957	2.153
P_{cb}^7	$\frac{1}{2}^+ \otimes 0^-$ $\frac{1}{2}^+ \otimes 1^-$	$\Xi_c B_s / \Xi'_c B_s, \Omega_c B$	7834 / 7945	$\frac{1}{2}(\frac{1}{2}^-)$	−0.380	0.362
			7883 / 7994	$\frac{1}{2}(\frac{1}{2}^-)$	−0.345	−0.465
				$\frac{1}{2}(\frac{3}{2}^-)$	−1.087	−0.154
P_{cb}^8	$\frac{1}{2}^+ \otimes 0^-$ $\frac{1}{2}^+ \otimes 1^-$	$\Xi_c B_s / \Xi'_c B_s, \Omega_c B$	7837 / 7945	$\frac{1}{2}(\frac{1}{2}^-)$	−0.956	0.362
			7886 / 7994	$\frac{1}{2}(\frac{1}{2}^-)$	0.999	−0.465
				$\frac{1}{2}(\frac{3}{2}^-)$	0.065	−0.154

octet representations, 8_{1f} and 8_{2f} . The results reveal a clear hierarchy. In the 8_{2f} representation, the $\frac{1}{2}^+ \otimes 0^-$ states display near–universal values, $\mu = -0.062 \mu_N$ for the entire $b\bar{c}$ octet and $\mu = +0.362 \mu_N$ for the $c\bar{b}$ octet, reflecting the spin–singlet light–di–quark structure that leaves the moment dominated by the heavy quark. The 8_{1f} representation, in contrast, exhibits a broad distribution of values with frequent sign changes. The inclusion of vector–meson components in the $\frac{1}{2}^+ \otimes 1^-$ configurations introduces strong spin–dependent effects and sign reversals, and the $J^P = \frac{3}{2}^-$ states systematically carry the largest magnitudes, making them the most favorable candidates for electromagnetic studies such as radiative transitions. The differences between the $b\bar{c}$ and $c\bar{b}$ families across all spin–parity assignments constitute direct evidence of heavy–quark flavor symmetry breaking in electromagnetic observables. Although direct measurements of static moments are challenging for short–lived pentaquarks, radiative widths and production asymmetries at LHCb, Belle II, and the Electron–Ion Collider could provide indirect access, and the benchmarks presented here should help guide such searches.

ACKNOWLEDGMENT

This work is supported by Scientific Research Projects Coordination Unit of Ondokuz Mayıs University with project BAP05-2025-5384, and also supported in part by the National Natural Science Foundation of China under Project

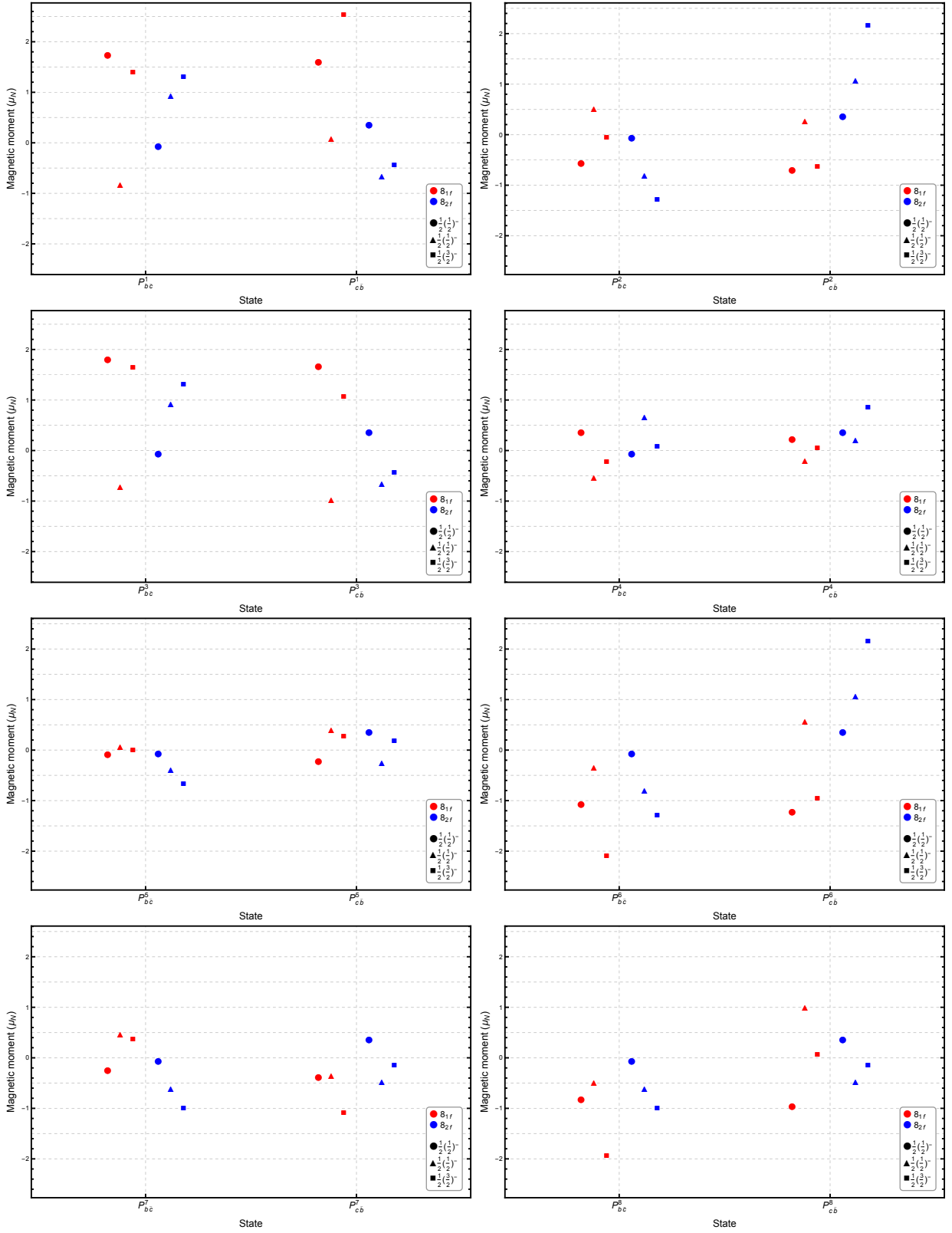


FIG. 1. Magnetic moments of the open bottom–charm molecular pentaquark octets $b\bar{c}$ and $\bar{c}b$ in the 8_{1f} and 8_{2f} flavor representations. The results are shown for the $J^P = \frac{1}{2}^-$ ($\frac{1}{2}^+ \otimes 0^-$ and $\frac{1}{2}^+ \otimes 1^-$) and $J^P = \frac{3}{2}^-$ ($\frac{1}{2}^+ \otimes 1^-$) configurations, with magnetic moments expressed in units of the nuclear magneton μ_N . The red color refers to 8_{1f} representation while the blue color refers to the 8_{2f} representation. The spin-parity configurations in Eq. (10) are denoted by circle, triangle, and square, respectively.

No. 12275023.

-
- [1] R. Aaij *et al.* (LHCb), Observation of $J/\psi p$ Resonances Consistent with Pentaquark States in $\Lambda_b^0 \rightarrow J/\psi K^- p$ Decays, *Phys. Rev. Lett.* **115**, 072001 (2015), [arXiv:1507.03414 \[hep-ex\]](#).
- [2] R. Aaij *et al.* (LHCb), Observation of a narrow pentaquark state, $P_c(4312)^+$, and of two-peak structure of the $P_c(4450)^+$, *Phys. Rev. Lett.* **122**, 222001 (2019), [arXiv:1904.03947 \[hep-ex\]](#).
- [3] T. Gershon (LHCb), Exotic hadron naming convention [10.17181/CERN.7XZO.HPH7](#) (2022), [arXiv:2206.15233 \[hep-ex\]](#).
- [4] R. Aaij *et al.* (LHCb), Evidence of a $J/\psi\Lambda$ structure and observation of excited Ξ^- states in the $\Xi_b^- \rightarrow J/\psi\Lambda K^-$ decay, *Sci. Bull.* **66**, 1278 (2021), [arXiv:2012.10380 \[hep-ex\]](#).
- [5] I. Adachi *et al.* (Belle, Belle-II), Search for $P_{cs}(4459)$ and $P_{cs}(4338)$ in Upsilon(1S,2S) inclusive decays at Belle, *Phys. Rev. Lett.* **135**, 041901 (2025), [arXiv:2502.09951 \[hep-ex\]](#).
- [6] R. Aaij *et al.* (LHCb), Observation of a $J/\psi\Lambda$ Resonance Consistent with a Strange Pentaquark Candidate in $B \rightarrow J/\psi\Lambda p^-$ Decays, *Phys. Rev. Lett.* **131**, 031901 (2023), [arXiv:2210.10346 \[hep-ex\]](#).
- [7] R. Chen, J. He, and X. Liu, Possible strange hidden-charm pentaquarks from $\Sigma_c^{(*)}\bar{D}_s^*$ and $\Xi_c^{(\prime,*)}\bar{D}^*$ interactions, *Chin. Phys. C* **41**, 103105 (2017), [arXiv:1609.03235 \[hep-ph\]](#).
- [8] B. Wang, L. Meng, and S.-L. Zhu, Spectrum of the strange hidden charm molecular pentaquarks in chiral effective field theory, *Phys. Rev. D* **101**, 034018 (2020), [arXiv:1912.12592 \[hep-ph\]](#).
- [9] M.-J. Yan, F.-Z. Peng, M. Sánchez Sánchez, and M. Pavon Valderrama, $P\psi s\Lambda(4338)$ pentaquark and its partners in the molecular picture, *Phys. Rev. D* **107**, 074025 (2023), [arXiv:2207.11144 \[hep-ph\]](#).
- [10] G.-J. Wang, R. Chen, L. Ma, X. Liu, and S.-L. Zhu, Magnetic moments of the hidden-charm pentaquark states, *Phys. Rev. D* **94**, 094018 (2016), [arXiv:1605.01337 \[hep-ph\]](#).
- [11] E. Ortiz-Pacheco, R. Bijker, and C. Fernández-Ramírez, Hidden charm pentaquarks: mass spectrum, magnetic moments, and photocouplings, *J. Phys. G* **46**, 065104 (2019), [arXiv:1808.10512 \[nucl-th\]](#).
- [12] Y.-J. Xu, Y.-L. Liu, and M.-Q. Huang, The magnetic moment of $P_c(4312)$ as a $\bar{D}\Sigma_c$ molecular state, *Eur. Phys. J. C* **81**, 421 (2021), [arXiv:2008.07937 \[hep-ph\]](#).
- [13] U. Özdem, Magnetic dipole moments of the hidden-charm pentaquark states: $P_c(4440)$, $P_c(4457)$ and $P_{cs}(4459)$, *Eur. Phys. J. C* **81**, 277 (2021), [arXiv:2102.01996 \[hep-ph\]](#).
- [14] M.-W. Li, Z.-W. Liu, Z.-F. Sun, and R. Chen, Magnetic moments and transition magnetic moments of P_c and P_{cs} states, *Phys. Rev. D* **104**, 054016 (2021), [arXiv:2106.15053 \[hep-ph\]](#).
- [15] U. Özdem, Electromagnetic properties of $D^-(*)\Xi c'$, $D^-(*)\Lambda c$, $D^-s(*)\Lambda c$ and $D^-s(*)\Xi c$ pentaquarks, *Phys. Lett. B* **846**, 138267 (2023), [arXiv:2303.10649 \[hep-ph\]](#).
- [16] U. Özdem, Investigation of magnetic moment of $P_{cs}(4338)$ and $P_{cs}(4459)$ pentaquark states, *Phys. Lett. B* **836**, 137635 (2023), [arXiv:2208.07684 \[hep-ph\]](#).
- [17] F. Gao and H.-S. Li, Magnetic moments of hidden-charm strange pentaquark states*, *Chin. Phys. C* **46**, 123111 (2022), [arXiv:2112.01823 \[hep-ph\]](#).
- [18] F. Guo and H.-S. Li, Analysis of the hidden-charm pentaquark states based on magnetic moment and transition magnetic moment, *Eur. Phys. J. C* **84**, 392 (2024), [arXiv:2304.10981 \[hep-ph\]](#).
- [19] F.-L. Wang, S.-Q. Luo, H.-Y. Zhou, Z.-W. Liu, and X. Liu, Exploring the electromagnetic properties of the $\Xi c^{(\prime,*)}D^-s^*$ and $\Omega c^{(\prime,*)}D^-s^*$ molecular states, *Phys. Rev. D* **108**, 034006 (2023), [arXiv:2210.02809 \[hep-ph\]](#).
- [20] F.-L. Wang, H.-Y. Zhou, Z.-W. Liu, and X. Liu, What can we learn from the electromagnetic properties of hidden-charm molecular pentaquarks with single strangeness?, *Phys. Rev. D* **106**, 054020 (2022), [arXiv:2208.10756 \[hep-ph\]](#).
- [21] U. Özdem, Analysis of the isospin eigenstate $\bar{D}\Sigma_c$, $\bar{D}^*\Sigma_c$, and $\bar{D}\Sigma_c^*$ pentaquarks by their electromagnetic properties, *Eur. Phys. J. C* **84**, 769 (2024), [arXiv:2401.12678 \[hep-ph\]](#).
- [22] H.-S. Li, F. Guo, Y.-D. Lei, and F. Gao, Magnetic moments and axial charges of the octet hidden-charm molecular pentaquark family, *Phys. Rev. D* **109**, 094027 (2024), [arXiv:2401.14767 \[hep-ph\]](#).
- [23] H.-S. Li, Molecular pentaquark magnetic moments in heavy pentaquark chiral perturbation theory, *Phys. Rev. D* **109**, 114039 (2024), [arXiv:2401.14759 \[hep-ph\]](#).
- [24] U. Özdem, Probing the electromagnetic structure of the $P_c(4337)^+$ pentaquark: insights from a diquark–diquark–antiquark picture for $J^P = \frac{1}{2}^-$ and $\frac{3}{2}^-$ states, *Eur. Phys. J. C* **85**, 704 (2025), [arXiv:2506.04345 \[hep-ph\]](#).
- [25] U. Özdem, Electromagnetic tomography of spin- $\frac{3}{2}$ hidden-charm strange pentaquarks, *JHEP* **02**, 207, [arXiv:2510.26893 \[hep-ph\]](#).
- [26] H. Mutuk, Magnetic moments of hidden-bottom pentaquark states, *Eur. Phys. J. C* **84**, 874 (2024), [arXiv:2403.16616 \[hep-ph\]](#).
- [27] H. Mutuk and X.-W. Kang, Unveiling the structure of hidden-bottom strange pentaquarks via magnetic moments, *Phys. Lett. B* **855**, 138772 (2024), [arXiv:2405.07066 \[hep-ph\]](#).
- [28] J. Wu, Y.-R. Liu, K. Chen, X. Liu, and S.-L. Zhu, Hidden-charm pentaquarks and their hidden-bottom and B_c -like partner states, *Phys. Rev. D* **95**, 034002 (2017), [arXiv:1701.03873 \[hep-ph\]](#).

- [29] J.-X. Lin, H.-X. Chen, W.-H. Liang, W.-Y. Liu, and D. Zhou, Molecular pentaquark states with open charm and bottom flavors, *Eur. Phys. J. A* **60**, 15 (2024), [arXiv:2308.01007 \[hep-ph\]](#).
- [30] Z.-Y. Wang and Z.-W. Long, Prediction of $QQqqs^-$ molecular pentaquarks within the extended local hidden gauge approach, *Phys. Rev. D* **112**, 056029 (2025), [arXiv:2508.21474 \[hep-ph\]](#).
- [31] S. Navas *et al.* (Particle Data Group), Review of particle physics, *Phys. Rev. D* **110**, 030001 (2024).
- [32] Z.-C. Yang, Z.-F. Sun, J. He, X. Liu, and S.-L. Zhu, The possible hidden-charm molecular baryons composed of anti-charmed meson and charmed baryon, *Chin. Phys. C* **36**, 6 (2012), [arXiv:1105.2901 \[hep-ph\]](#).
- [33] M. Jacob and G. C. Wick, On the General Theory of Collisions for Particles with Spin, *Annals Phys.* **7**, 404 (1959).
- [34] R. Aaij *et al.* (LHCb), First Determination of the Spin-Parity of $\Xi_c(3055)^+,0$ Baryons, *Phys. Rev. Lett.* **134**, 081901 (2025), [arXiv:2409.05440 \[hep-ex\]](#).
- [35] X.-W. Kang, H.-B. Li, and B.-S. Zou, Partial wave analysis of $\psi' \rightarrow \gamma \chi(c0) \rightarrow \gamma p K^- \Lambda_c^-$ being used for searching for baryon resonance, *Chin. Phys. C* **34**, 1061 (2010), [arXiv:0911.2998 \[hep-ph\]](#).
- [36] X.-W. Kang, H.-B. Li, G.-R. Lu, and A. Datta, Study of CP violation in Λ_c^+ decay, *Int. J. Mod. Phys. A* **26**, 2523 (2011), [arXiv:1003.5494 \[hep-ph\]](#).
- [37] J. Charles, S. Descotes-Genon, X.-W. Kang, H.-B. Li, and G.-R. Lu, Extracting CP violation and strong phase in D decays by using quantum correlations in $\psi(3770) \rightarrow D0 D0\text{-bar} \rightarrow (V(1)V(2))(V(3)V(4))$ and $\psi(3770) \rightarrow D0 D0\text{-bar} \rightarrow (V(1)V(2))(K \pi)$, *Phys. Rev. D* **81**, 054032 (2010), [arXiv:0912.0899 \[hep-ph\]](#).
- [38] B. Wang, B. Yang, L. Meng, and S.-L. Zhu, Radiative transitions and magnetic moments of the charmed and bottom vector mesons in chiral perturbation theory, *Phys. Rev. D* **100**, 016019 (2019), [arXiv:1905.07742 \[hep-ph\]](#).